www.MaterialsViews.com

Highly Ordered Arrays of Femtoliter Surface Droplets

*Lei Bao, Amgad R. Rezk, Leslie Y. Yeo, and Xuehua Zhang**

The patterning of droplets in arrays on a solid surface is of significant interest, both from a fundamental standpoint of colloid and interface science, wetting, and thermodynamics,[1–6] as well as for a variety of applications across photonics and near-field imaging,[7,8] biomolecular, cell and tissue analysis,[9–12] high throughput drug screening,[13] DNA sequencing, and digital polymerase chain reaction.[14,15] The demand for increasingly smaller scale resolution, higher throughput processing, and greater detection sensitivity, however, has driven the need for further miniaturization to achieve smaller droplet volumes and denser array networks. This, in turn, has driven the development of techniques for droplet synthesis, including inkjet printing,[16] condensation-driven nucleation,[17] or droplet deposition on pre-patterned substrates.[18–21] Most of these techniques, however, allow patterning of the droplets only in air. There are nevertheless several advantages of patterning the droplets on a substrate immersed in an immiscible liquid medium, not least the extended droplet lifetimes due to lower dissolution rates and the elimination of evaporation in air, in addition to the possibility for controlling the droplet morphology by varying the surrounding liquid phase.[22]

Solvent exchange is one method by which a large quantity of droplets can be generated on an immersed substrate. In this method, a good solvent of oil (e.g., ethanol) is simply displaced by a poor solvent (e.g., water), such that the oversaturated oil precipitates to form droplets on the substrate.[23–26] Droplet formation during solvent exchange occurs via heterogeneous nucleation, following which the droplet grows through a diffusion-driven process in an oversaturated liquid.[26] This droplet formation process is fundamentally different from the droplet trapping method in which small volumes from a bulk flow are retained on surface microstructures due to their wettability in the interstitial spaces between the structures.[21] The nucleation and growth dynamics during the solvent exchange provide the unique possibility for controlling the final droplet size simply through the manipulation of macroscopic parameters (e.g., the solution concentration) during the droplet growth stage. Indeed, both the chemistry of the solutions and the flow conditions can potentially be exploited to manipulate the average droplet size on homogeneous substrates.[25,26] In particular, it has been demonstrated that the average droplet size can be tuned through global modulation of the concentration gradient in the solutions to produce droplet heights on the order 0.01–1 μm (and hence the term "mesoscale droplets") and droplet volumes in the 0.5–50 femtoliter (fL) range.[27] Nevertheless, the limitations to date with the solvent-exchange method has been the large distribution in the droplet sizes that are obtained and their random positioning on the substrate.[22] As such, this has constrained its practical use in applications where uniform droplet volumes, tunable droplet morphology, and precise positioning or large-scale patterning into ordered arrays are desirable.

We show in this work that it is possible to circumvent these limitations through selective nucleation, growth, and confinement of the droplets on arrays of smooth hydrophobic pre-patterned microdomains on the hydrophilic substrate. We observe the droplet volumes in the array to be highly uniform, their contact angles to be related to the dimension of the lateral confinement of the microdomains, and that it is possible to tune these by varying the saturation level in the bulk liquid. In addition to providing insight into the fundamental underlying mechanism responsible for control of the droplet morphology, we also demonstrate, as a proof-of-concept example application, a technique for the simple fabrication of low-cost and portable nanolens arrays for optical manipulation that is based on photopolymerization of the surface droplets.

Figure 1a–e, which comprise optical images of the polymerized droplets, show their spatial arrangement into highly ordered arrays on the pre-patterned substrates. The inter-droplet spacing, measured as the distance between the centers of two droplets, is observed to closely match that of the hydrophobic patterns, as shown in Figure S1 (Supporting Information). **Figure 2**a, on the other hand, shows the close one-to-one correlation between the average lateral diameter of the droplets and that of the patterns. Specifically, the lateral diameters of the polymerized droplets were measured to be 1.03 ± 0.12 μm, 2.93 ± 0.34 μm, 4.98 ± 0.14 μm, 9.86 ± 0.26 μm, and 28.9 ± 2.62 μm for pre-patterned arrays with diameters of 1 ± 0.10 μm, 3 ± 0.10 μm, 5 ± 0.11 μm, 10 ± 0.14 μm and 30 ± 0.20 μm, respectively. These results clearly confirm the formation of the droplets exclusively on the patterned hydrophobic microdomains as well as confinement of their lateral growth within the domain. It is therefore possible to not only precisely control the dimension, spacing, and location of the droplets, but also to control the droplet number, density, and spatial arrangement through the design of chemical patterns on the substrate surface.

Dr. L. Bao, Dr. A. R. Rezk, Prof. L. Y. Yeo, Prof. X. Zhang
School of Civil, Environmental, and Chemical Engineering
RMIT University
Melbourne, VIC 3001, Australia
E-mail: xuehua.zhang@rmit.edu.au

DOI: 10.1002/smll.201501105

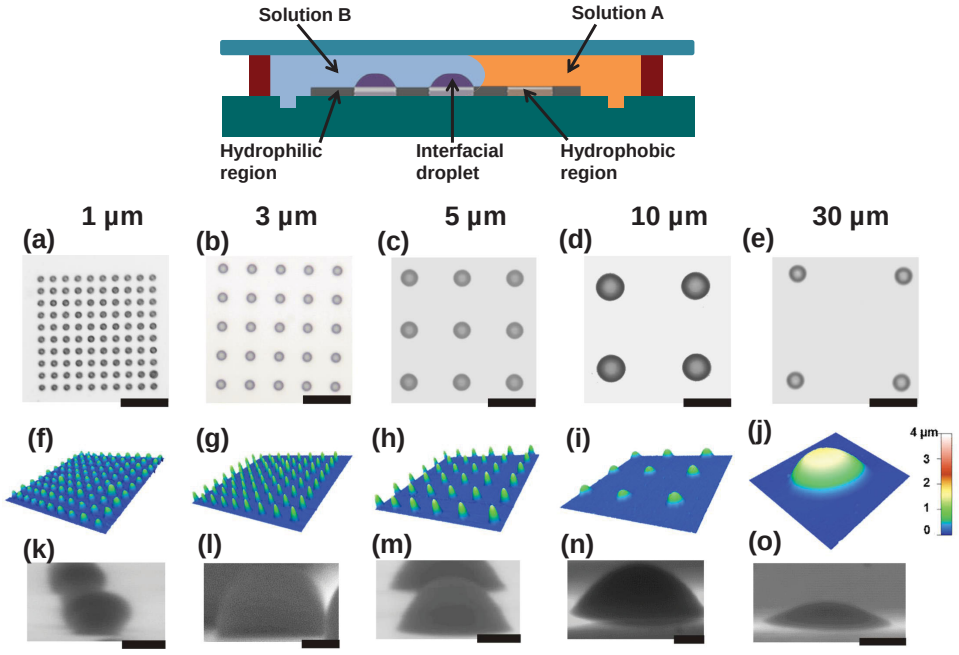

Figure 1. Illustration of the solvent exchange process (top image) and morphological characteristics of polymerized droplets on circular hydrophobic microdomains with diameters 1, 3, 5, 10 and 30 μm patterned on a silicon substrate (subsequent rows). The length of the scale bars in the optical images is 15 μm in panels (a)–(d) and 70 μm in panel (e). The dimensions of the AFM images are 30×30 μm^2 in panel (f) and 80×80 μm^2 in panels (g)–(j). The morphology of the polymerized droplets can be extracted reliably from the droplet heights in the AFM images in panels (f)–(j) and the lateral droplet dimensions in the SEM images in panels (k)–(o). The length of the scale bars is 1 μm in panels (k)–(l), 2 μm in panels (m)–(n) and 10 μm in panel (o).

To examine the dependence of the droplet contact angle and volume on the lateral dimension of the hydrophobic domains (Figure 2b,c), we carry out the solvent exchange simultaneously on both a homogeneous hydrophobic substrate and the pre-patterned substrates under identical solution conditions. As can be seen in Figure S2 (Supporting Information), large variation in the droplet lateral diameters were obtained on the homogeneous substrate, consistent with previous work on similar substrates wherein considerable polydispersity (standard deviations typically on the order of several microns) was observed in the droplets that were generated.[24] In contrast, fairly monodispersed droplet lateral diameter distributions were obtained with the pre-patterned hydrophobic microdomains in which the standard deviations are no greater than 200 nm, as shown in Figure 2a.

Further contrast between the homogeneous and pre-patterned substrates can be seen from measurements of the contact angles shown in Figure 2c. In particular, we observe the contact angle to be independent of the lateral droplet dimension for the homogeneous substrates, i.e., the droplet height and volume increased with its lateral size to maintain a contact angle of approximately 15°. In contrast, droplets that were formed on the hydrophobic domains possessed smaller contact angles as their lateral dimension increased. The former observation indicates that the droplets on the homogeneous substrates may grow mainly through a constant contact angle mode (CA), as illustrated by schematic I in the inset of Figure 2c.

The dependence of the contact angle on the lateral dimension of the pre-patterned microdomains, on the other hand, can be understood from the droplet formation mechanism by solvent exchange, wherein the surface droplets form by heterogeneous nucleation at the solid–liquid interface and subsequently expand via a diffusion-driven growth process.[6] While initial growth may occur via a CA mode when the lateral diameters of nucleated droplets are smaller than the domain size, subsequent growth occurs via a constant contact area mode (or constant contact radius mode CR) when the droplets reach and are confined by the domain boundaries of the patterns, as illustrated by schematic II. Consequently, the restriction of the lateral expansion of the droplets due to the hydrophobic microdomain boundaries then causes an increase in the droplet height as long as it keeps growing until the solvent exchange process is exhausted.

To first approximation, we thus neglect the initial CA mode transient and only focus on the model the droplet growth on different domain sizes under CR conditions as it is this latter growth that determines the final height and contact angle of the droplets. In the CR mode, the growth of the droplet and hence the evolution of its contact angle θ with time t is given by[22]

$$\frac{\mathrm{d}\theta}{\mathrm{d}t} = \frac{4D}{D_\mathrm{d}^2}\frac{C_\mathrm{s}}{\rho}(1+\cos\theta)^2 f(\theta)\xi, \tag{1}$$

where

$$\int_0^{\theta f} \frac{\mathrm{d}\theta}{f(\theta)(1+\cos\theta)^2} = \int_0^t \frac{4D}{D_\mathrm{d}^2}\frac{C_s}{\rho}\xi \mathrm{d}t \tag{2}$$

and

www.MaterialsViews.com

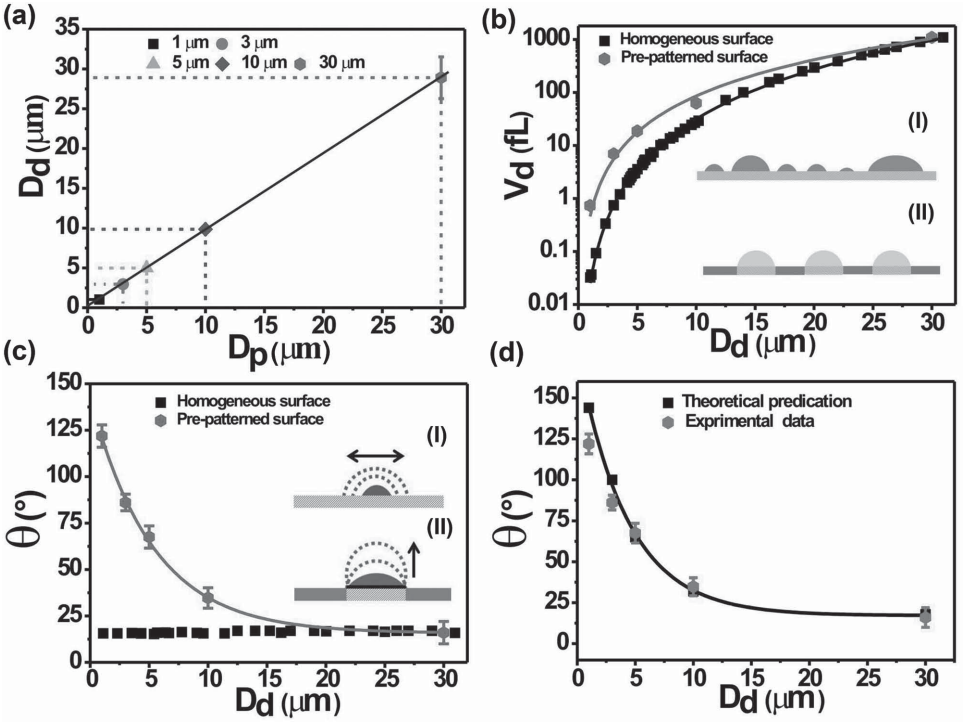

Figure 2. Size and morphological characteristics of the polymerized droplets formed on the pre-patterned hydrophobic substrates compared with those generated on homogeneous hydrophobic substrates. (a) Dependence of the lateral droplet diameter D_d on the diameter of the pre-patterned hydrophobic microdomains D_p. The plots in (b) and (c) show the droplet volume V_d and contact angle θ, respectively, as a function of D_d on the pre-patterned and homogeneous substrates. The schematic in (b) illustrates (I) the polydispersity of the droplets on the homogeneous substrate and (II) the uniform size distribution of the droplets on the pre-patterned substrates. The schematic in (c) illustrates droplet growth via (I) a constant contact angle mode on the homogeneous substrate and the initial stages on the pre-patterned substrate, as opposed to (II) a constant contact area mode in the latter stages on the pre-patterned substrate once the droplet is pinned on the domain boundary of the patterns. (d) Comparison between the theoretical prediction obtained from a constant contact area model with the experimental measurements of θ as a function of D_d. All trend lines were added to aid visualization.

$$\xi = C_\infty / C_S - 1 \tag{3}$$

In the above, D is the diffusion coefficient (6.5×10^{-10} m^2 s^{-1}), ρ is the density of the liquid droplet (1202 kg m^{-3}), C_s is the solubility of oil in the solution, and ξ the oversaturation level of oil in the solution. We note that during the solvent exchange, C_s and ξ are dependent on the composition in the liquid phase. However, given that the droplets were produced under identical liquid and flow conditions, C_s and ξ are assumed to be constant at a given value of t across all experiments with different microdomain pattern dimensions. Here, we assume values of 0.0343 g/100 g (approximating the solubility of HDODA in water) for C_s and 0.43 for ξ at $t \approx 2$ s. Numerically integrating Equations (1) and (2) for the droplets with lateral diameters D_d equal to the size of the domains D_p then gives theoretical predictions for the initial and final contact angle θ_f plotted in Figure 2d, which are in a good agreement with the experimental data across the different domain sizes. We note that the slight overestimation in the contact angle for the small 1 μm patterns, which may be due to the limitation of Equation (1) to small contact angles.[28] Additionally, there exists an upper limit in the contact angle that is imposed by the surface wettability of the hydrophilic region surrounding the hydrophobic microdomains[18] wherein the contact angle of the pinned droplet cannot exceed the macroscopic contact angle of the droplets on hydrophobic surfaces in water,[29] which is measured to be approximately 118°.

In any case, such dependence of the contact angle and hence the height of the droplets together with the droplet volume in the CR mode offers additional flexibility and ease for tuning the droplets during the solvent exchange process to a desired morphology for a particular application. For example, given that the mass gain of the droplet is proportional to the oversaturation in the liquid phase ξ in Equation (2), it is possible to tune the volume and morphology of the droplets simply through ξ, i.e., by varying the saturation level (i.e., the concentration) of oil in solution A. **Figure 3** shows the morphology (panels (a)–(h)) and height (panels (i)–(l)) of the polymerized droplets at two representative oil concentrations (more AFM images are provided in Figure S3 in the Supporting Information). The plots of the droplet volume and contact angle (panels (m) and (n), respectively, in Figure 3) as a function of the concentration summarize the morphology of the droplets formed at three different oil concentrations including those in Figure 1. In particular, the average droplet volume is seen to increase and its contact angle to decrease with increasing domain sizes for all concentrations, consistent with that observed previously. For a fixed pattern dimension, however, the droplet contact angle and volume are observed to decrease with decreasing oil concentration in the solution. Of note is the possibility of decreasing the droplet volume to

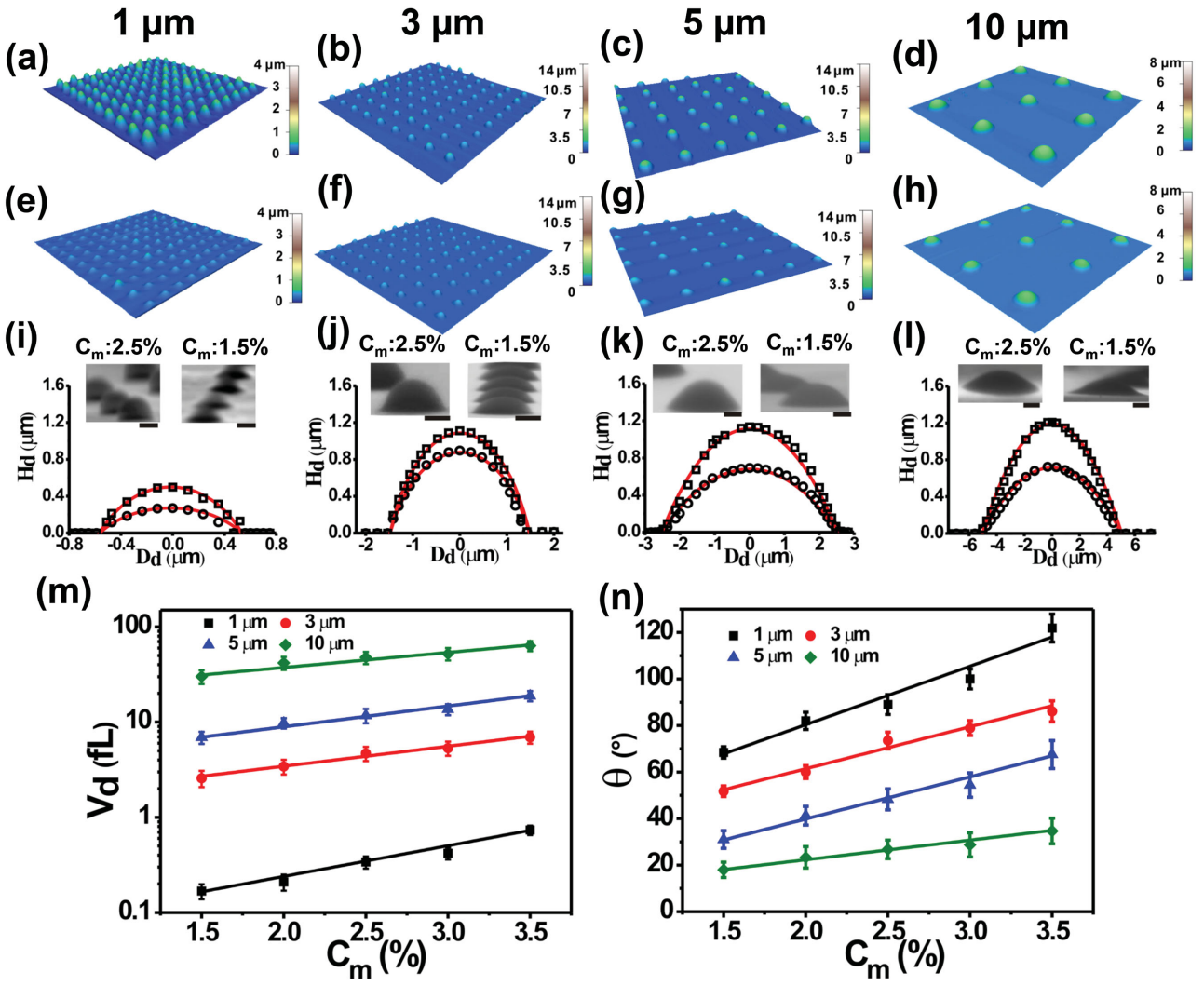

Figure 3. Morphology and size of the polymerized droplets formed on pre-patterned hydrophobic substrates at five different oil concentrations C_m. (a)–(i) show AFM images and cross-sectional profiles of the polymerized droplets at two representative concentrations. (a)–(d): C_m = 2.5% (square points in panels (i)–(l)); (e)–(h): C_m = 1.5% (circles in panels (i)–(l)). In panels (i)–(l), the solid curves represent idealized spherical caps; the length of the scale bars for the SEM images is 0.5 μm in panels (i), 1 μm in panels (j),(k) and 2 μm in panels (l). The plots show the volume (m) and the contact angle (n) of the polymerized droplets as a function of the oil concentration, C_m. The trend lines in panels (m) and (n) are added to aid visualization.

ca. 1.6 attoliters simply by decreasing the oil concentration from 3.5% to 1.5%.

As proof-of-concept of an exemplary application, we briefly demonstrate the possibility of exploiting this femtoliter droplet generation technique as a simple and low-cost method for fabricating portable nanolens arrays. Following the process illustrated in **Figure 4**a, we first produced the polymerized droplet (i.e., the nanolenses) arrays on the pre-patterned silicon substrates, followed by poly(dimethylsiloxane) (PDMS) casting over the substrate. After curing the PDMS, we then carefully peeled the transparent PDMS film together with the nanolens array off the substrate to form a freestanding transparent membrane, while preserving the highly ordered arrangement of the nanolens. To test for its optical properties, the PDMS film with the embedded nanolens array was subsequently illuminated by a beam of white light normal to the film through a 0.5 mm pinhole, resulting in the domain-size-dependent diffraction patterns shown in Figure 4b when projected onto a sheet of white paper. This simple demonstration of the utility of these highly ordered droplet arrays produced via solvent exchange, together with the possibility for controlling the nanolens structure through tunability of the morphology of the droplet precursors, then opens up new low-cost and portable alternatives for photonic manipulation, for example, for enhancing light harvesting wherein the diffraction of light through a microlens layer has been shown to reduce loss of intensity in solar cells.[8,30] Additionally, these submillimeter thin PDMS films could also find widespread application as low-cost screen coatings in portable consumer devices.

In summary, we demonstrate the possibility of generating highly ordered arrays of femtoliter and sub-femtoliter volume droplets on a pre-patterned substrate immersed under an aqueous solution through a nucleation-and-growth process triggered simply by solvent exchange. Given the confinement of the lateral growth of the droplets by the boundaries of

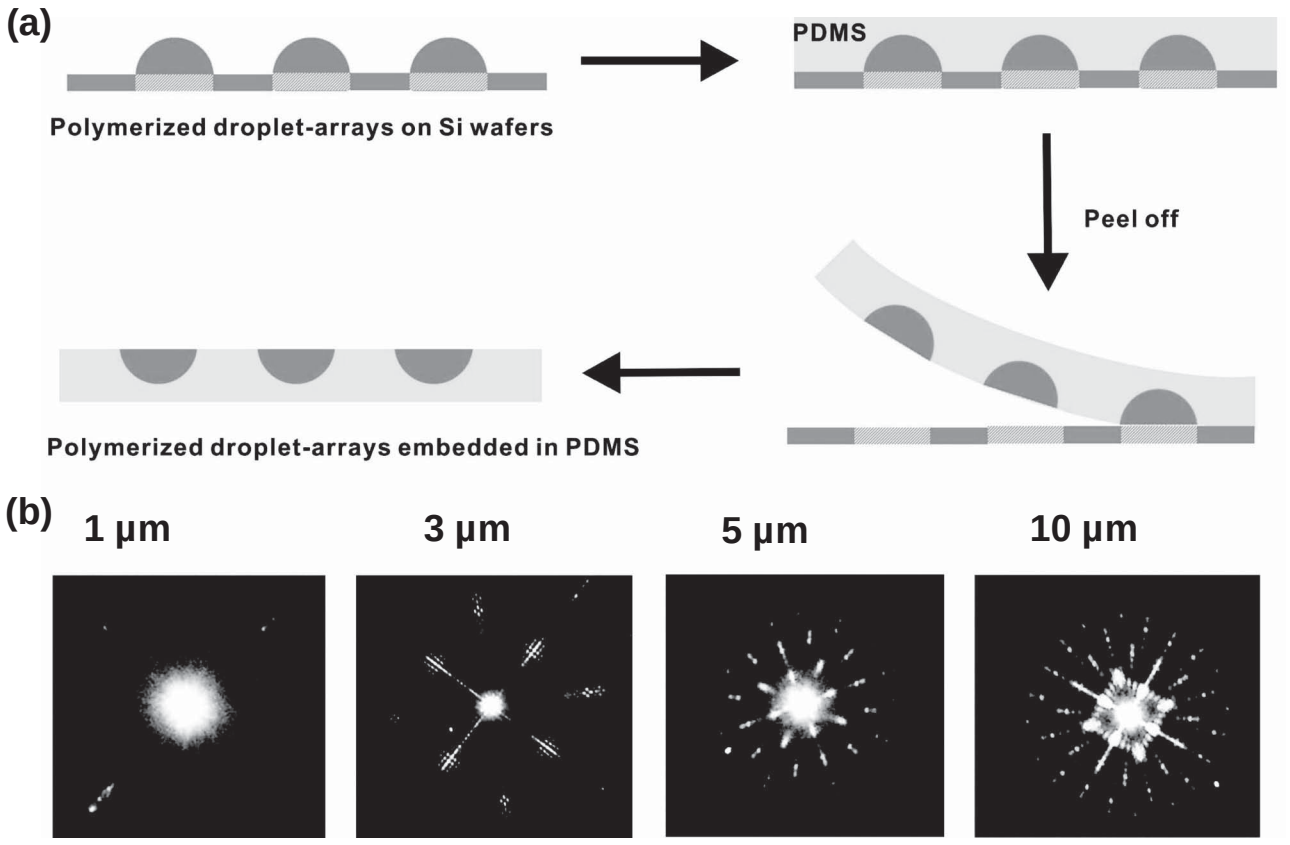

Figure 4. (a) Schematic illustration of the process for fabricating a simple and portable nanolens array. The droplets were produced on prepatterned silicon substrates, followed by their polymerization into nanolenses. PDMS was subsequently cast on the substrate, and the nanolens array embedded in the PDMS film was then be peeled off the substrate to form a freestanding structure. (b) Resulting diffraction patterns when a beam of white light is projected normal to the transparent PDMS film.

the smooth hydrophobic microdomain patterns, the volume and contact angle of the droplets in the patterned arrays are shown to be closely related to their lateral dimension and hence that of the patterns. The final contact angle of the droplets in the arrays is in agreement with a theoretical prediction for the diffusion-driven droplet growth under a constant contact area mode. Such control of the droplet volume and morphology, for example, simply by altering the oil saturation level in the solution, together with the possibility for precise regulation of the size, number density, and positioning of the droplets, then offers extensive opportunities for tuning these arrays for a desired application. As but one example across many possible applications, we show how these arrays can be exploited for fabricating low-cost and portable nanolens arrays embedded in a transparent polymer film for potential use for photonic manipulation.

Experimental Section

Fabrication of Hydrophobic Microdomains on Hydrophilic Substrates: To prepare the pre-patterned substrates, photoresist (AZ1512HS, MicroChemicals GmbH, Ulm, Germany) was spun coated on silicon wafers (University Wafer Inc., Boston, MA) precleaned in piranha solution (30% H_2O_2, 70% H_2SO_4), and subsequently exposed to UV light through a photomask. After rinsing the substrates in developer solution and DI water, the unprotected circular domains were exposed and chemically modified by octadecyltrimethylchlorosilane (OTS; >90%; Sigma–Aldrich Corp., St. Louis, MO), resulting in circular hydrophobic domains with diameters ranging from 1 to 30 μm. The hydrophilic background was then exposed by removal of the photoresist coating on the Si/SiO_2 substrate. The average roughness of the OTS-coated microdomains is below 2 nm and the contact angles of water in air on the hydrophilic and hydrophobic domains were found to be 10° and 118°, respectively.

Formation of Droplet Arrays on the Prepatterned Surface: Interfacial femtodroplet microarrays were then produced on the surface of the chemically patterned hydrophobic/hydrophilic substrates through solvent exchange, [24–25,27] as illustrated in the schematic in Figure 1. Briefly, the chemically patterned substrate was placed inside a fluid chamber through which two solutions were flowed: solution A comprising 50% ethanol–water solution with 1.5%–3.5% 1,6-hexanediol diacrylate (HDODA; Sigma–Aldrich Corp., St Louis, MO), and solution B comprising HDODA-saturated water. Solution A was first injected into the chamber followed by solution B, which displaced solution A at a constant flow rate of 200 μL min^{-1} to form droplets of HDODA.

At the end of the solvent exchange, we injected solution B with 0.04 vol% dissolved photoinitiator (2-hydroxy-2-methylpropiophenone; Sigma-Aldrich Corp., St. Louis, MO) and polymerized the droplets under UV irradiation. The morphology of polymerized

small NANO MICRO

droplets—characterized using reaction-mode optical microscopy (Huvitz HRM-300, Scitech Pty. Ltd., Preston, VIC, Australia), atomic force microscopy (AFM; Asylum Research, Santa Barbara,CA) and scanning electronic microscopy (SEM; Quanta 200 ESEM, FEI, Hillsboro, OR)—were used to represent that of the interfacial droplets[31] as it is nontrivial to obtain reliable morphology of those highly deformable droplets in liquid from direct AFM imaging.[32,33] Here the contact angle and volume of the droplets were calculated from fitting spherical caps with their height and lateral diameter measured from AFM and SEM images of the polymerized droplets. The buoyancy had no effect on the droplet morphology due to their very small volumes. To test the optical properties, the polymerized droplets were embedded into a thin film of PDMS (Sigma–Aldrich Corp., St. Louis, MO) and peeled off the substrate.

Supporting Information

Supporting Information is available from the Wiley Online Library or from the author.

Acknowledgements

The authors thank Detlef Lohse for his advice on the model and for very stimulating discussions. X.H.Z and L.Y.Y acknowledge support from the Australian Research Council through the Future Fellowship (FT120100473, FT130100672) and Discovery Project (DP140100805) schemes. L.B. is grateful to the Australian Government (Department of Education and Training) for an Endeavour Research Fellowship. The authors also acknowledge the use of facilities and the associated technical support at the RMIT Micro-Nano Reserach Facility and the Microscopy and Microanalysis Facility.

[1] P. G. de Gennes, F. Brochard-Wyart, D. Quéré, *Capillarity and Wetting Phenomena: Drops, Bubbles, Pearls, Waves*, Springer, New York **2004**.
[2] D. Quéré, *Nat. Mater.* **2004**, *3*, 79.
[3] D. Quéré, *Annu. Rev. Mater. Res.* **2008**, *38*, 71.
[4] A. Mendez-Vilas, A. B. Jodar-Reyes, M. L. Gonzalez-Martin, *Small* **2009**, *5*, 1366.
[5] F. Eslami, J. A. W. Elliott, *J. Phys. Chem. B.* **2014**, *118*, 3630.
[6] D. Lohse, X. H. Zhang, *Rev. Mod. Phys.* **2015**, unpublished.
[7] Z. B. Wang, W. Guo, L. Li, B. Luk'yanchuk, A. Khan, Z. Liu, Z. Chen, M. H. Hong, *Nat Commun.* **2011**, *2*, 218.
[8] Y. Q. Chen, M. Elshobaki, R. Gebhardt, S. Bergeson, M. Noack, J.-M. Park, A. C. Hillier, K.-M. Ho, R. Biswas, S. Chaudhary, *Phys. Chem. Chem. Phys.* **2015**, *17*, 3723.
[9] J. Ziauddin, D, M. Sabatini, *Nature* **2001**, *411*, 107.
[10] C. J. Flaim, S. Chien, S. N. Bhatia, *Nat. Methods* **2005**, *2*, 119.
[11] H. Z. Li, Q. Yang, G. N. Li, M. Z. Li, S. T. Wang, Y. L. Song, *ACS Appl. Mater. Interfaces* **2015**, *7*, 9060.
[12] J. Hou, H. C. Zhang, Q. Yang, M. Z. Li, Y. L. Song, L. Jiang, *Angew. Chem. Int. Ed.* **2014**, *53*, 5791.
[13] J. G. Hong, J. B. Edel, A. J. de Mello, *Drug Discovery Today* **2009**, *14*, 134.
[14] A. Maitra, Y. Cohen, S. E. D. Gillespie, E. Mambo, N. Fukushima, M. O. Hoque, N. Shah, M. Goggins, J. Califano, D. Sidransky, A. Chakravarti, *Genome Res.* **2004**, *14*, 812.
[15] N. Shao, S.-M. Jiang, M. Zhang, J. Wang, S.-J. Guo, Y. Li, H.-W. Jiang, *Anal. Chem.* **2014**, *86*, 1269.
[16] M. X. Kuang, L. B. Wang, Y. L. Song, *Adv. Mater.* **2014**, *24*, 6950.
[17] Y. Yamada, T. Ikuta, T. Nishiyama, K. Takahashi, Y. Takata, *Langmuir* **2014**, *30*, 14532.
[18] L. Wang, T. J. McCarthy, *Proc. Natl. Acad. Sci. USA* **2015**, *112*, 2664.
[19] A. P. Fang, E. Dujardin, T. Ondarçuhu, *Nano Lett.* **2006**, *6*, 2368.
[20] A. Verma, A. Sharma, *Adv. Mater.* **2010**, *22*, 5306.
[21] S. Sakakihara, S. Araki, R. Iino, H. Noji, *Lab Chip* **2010**, *10*, 3355.
[22] X. H Zhang, J. Wang, L. Bao, E. Dietrich, R. C. A. van der Veen, S. H. Peng, J. Friend, H. J. W. Zandvliet, L. Yeo, D. Lohse, *Soft Matter* **2015**, *11*, 1889.
[23] S. T. Lou, Z. Q. Ouyang, Y. Zhang, X. J. Li, J. Hu, M. Q. Li, F. J. Yang, *J. Vac. Sci. Technol. B* **2000**, *18*, 2573.
[24] H. J. Yang, S. H. Peng, X. T. Hao, T. A. Smith, G. G. Qiao, X. H. Zhang, *Soft Matter* **2014**, *10*, 957.
[25] X. H. Zhang, W. Ducker, *Langmuir* **2007**, *23*, 12478.
[26] X. H. Zhang, Z. Y. Lu, H. S. Tan, L. Bao, Y. H. He, C. Sun, D. Lohse, unpublished.
[27] X. H. Zhang, J. M. Ren, H. J. Yang, Y. H. He, J. F. Tan, G. G. Qiao, *Soft Matter* **2012**, *8*, 4314.
[28] Y. O. Popov, *Phys. Rev. E* **2005**, *71*, 036313.
[29] A. Valencia, R. Lipowsky, *Langmuir* **2004**, *20*, 1986.
[30] Y. Q. Chen, M. Elshobaki, Z. Ye, J.-M. Park, M. A. Noack, K.-M. Ho, S. Chaudhary, *Phys. Chem. Chem. Phys.* **2013**, *15*, 4297.
[31] Strictly speaking, the volume of the liquid droplet prior to polymerization is about 20% larger than that of its polymerized form due to the increase in density as it is polymerized.
[32] X. H. Zhang, W. Ducker, *Langmuir* **2008**, *24*, 110.
[33] A. Brotchie, X. H. Zhang, *Soft Matter* **2011**, *7*, 265.

Received: April 21, 2015
Revised: May 13, 2015
Published online: July 14, 2015

